Semiconductor Physics, Quantum Electronics & Optoelectronics, 2025. V. 28, No 1. P. 010-018.

Semiconductor physics

Ferroelectric nanoparticles in liquid crystals: Role of ionic transport at small nanoparticle concentrations

Ju.M. Gudenko[1], O.S. Pylypchuk[1], V.V. Vainberg[1], I.A. Gvozdovskyy[1], S.E. Ivanchenko[2], D.O. Stetsenko[1], N.V. Morozovsky[1], V.N. Poroshin[1], E.A. Eliseev[2*], and A.N. Morozovska[1]**

[1]Institute of Physics, National Academy of Sciences of Ukraine,
46 Nauky Avenue, 03028 Kyiv, Ukraine
[2]Frantsevich Institute for Problems in Materials Science, National Academy of Sciences of Ukraine,
3 Omeliana Pritsaka Street, 03142 Kyiv, Ukraine
Corresponding author e-mail: eugene.a.eliseev@gmail.com[*], anna.n.morozovska@gmail.com[**]

Abstract. We reveal an apparent influence of ultra-small concentrations (1 wt.% or less) of $BaTiO_3$ nanoparticles (average size of 24 nm) on the current-voltage characteristics and capacitance of dielectric liquid crystal (LC) 5CB. A pure LC cell demonstrates higher current (and, hence, smaller resistance) as compared to LC cells filled with very small concentrations (0.5 and 1 wt.%) of $BaTiO_3$ nanoparticles. The same trend is observed for the charge-voltage characteristics: the capacitance loop is the widest for the pure LC cell and becomes noticeably thinner in the presence of 0.5 and 1 wt.% of $BaTiO_3$ nanoparticles. This seems counterintuitive, because 1 wt.% of ferroelectric nanoparticles modify the effective dielectric response very slightly and therefore should not influence on the director distribution and elastic properties of the LC. We conclude that a possible physical reason of this observation is the influence on the ionic transport in the LC of the ionic-electronic screening charges, which cover the ferroelectric nanoparticles and become polarized in an external field.

Keywords: dielectric liquid crystal, ferroelectric nanoparticles, $BaTiO_3$ nanoparticles, current-voltage characteristics, ionic transport.

https://doi.org/10.15407/spqeo28.01.010
PACS 73.63.–b, 73.63.Kv, 77.84.Nh, 77.84.–s.

Manuscript received 25.09.24; revised version received 04.02.25; accepted for publication 12.03.25; published online 26.03.25.

1. Introduction

Experimental implementation of ferroelectric nanoparticles (NPs) is abundant (see *e.g.* [1–5]), and the NP sizes of 5 to 50 nm are typical experimental values [6–9]. There are several studies that use ferroelectric NPs fabricated in heptane and core-shell nanoparticles produced using oleic acid [7, 10–13].

Ferroelectric NPs are very important for advanced optical, optoelectronic, and chemical applications [8–14, 15]. In the experimental papers [7, 10, 11, 15], particles suspended in a liquid dielectric medium were studied. These core-shell NPs exhibited spontaneous polarization up to 130 $\mu C/cm^2$ [7, 11, 16]. Ferroelectric and paraelectric nanoparticles can significantly influence on phase transitions and dynamics in nematic liquid crystals [12]. Despite the advances of using such NPs, many aspects of their preparation technology [17] and fundamental understanding of their properties [18–20] are still a challenge. In this context, small $BaTiO_3$ NPs embedded in liquid or polymer matrices are of permanent scientific interest [21–23].

This work studies the influence of very small concentrations (1 wt.% or less) of $BaTiO_3$ NPs (average size of 24 nm) on the current-voltage and charge-voltage characteristics, dielectric permittivity and losses of a dielectric liquid crystal 5CB.

2. Experimental

2.1. Sample preparation

To study the influence of nanoparticles on the current-voltage characteristics, symmetrical liquid crystal (LC) cells filled with pure nematic LC 5CB and liquid crystalline suspension based on $BaTiO_3$ (BTO) NPs dissolved in the 5CB were used. First, glass substrates (microscope slides made in Germany) were coated with thin ITO ($(In_2O_3)_{0.9}$–$(SnO_2)_{0.1}$) layers (see Fig. 1a). A 10:1 n-menthyl-2-pyrrolidone solution of PI2555 (HD MicroSystems, USA) [24] was deposited onto the glass substrates with the ITO layers and spin-coated (6800 rpm during 10 s) to obtain a thin aligning film as shown in Fig. 1b. The substrates were dried at 80 °C for 15 min followed by thermo-polymerization of polyimide

© V. Lashkaryov Institute of Semiconductor Physics of the NAS of Ukraine, 2025
© Publisher PH "Akademperiodyka" of the NAS of Ukraine, 2025

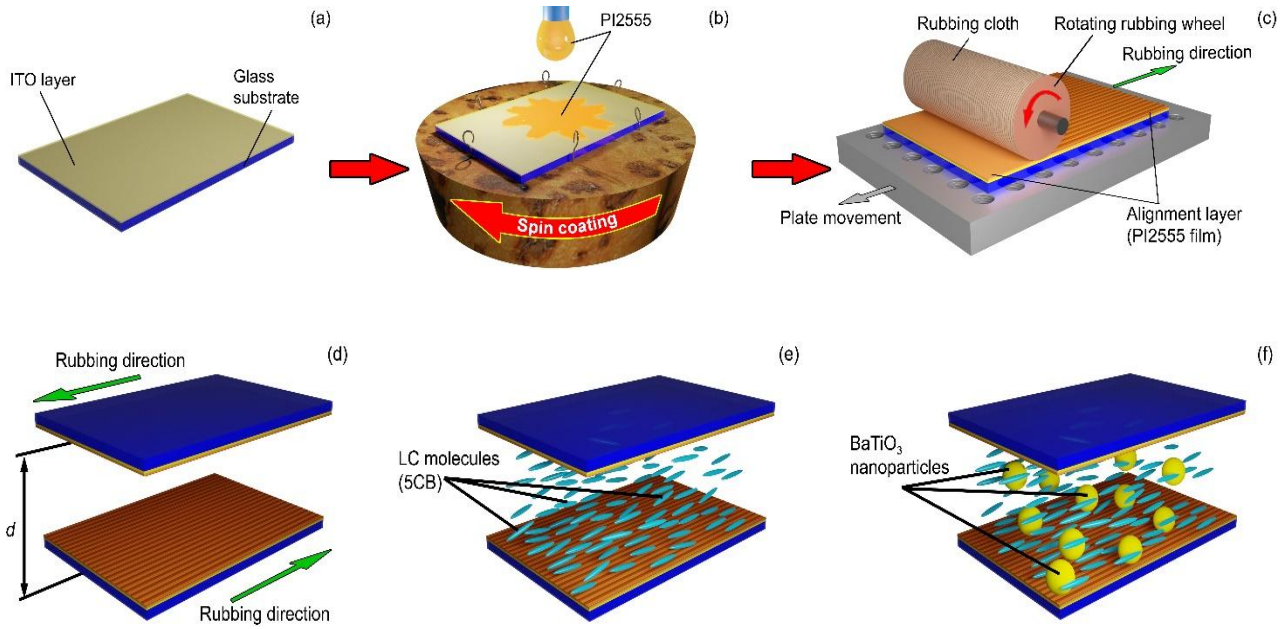

Fig. 1. Schematic illustration of LC cell preparation stages (a)–(d), the LC cell (e) and the LC cell with BTO NPs (f).

molecules at 180 °C during 30 min. The PI2555 film was rubbed $N_{rubb} = 15$ times (Fig. 1c) to achieve high value of azimuthal anchoring energy of about 10^{-5} J/m^2 [25].

The LC cells were assembled of two rubbed substrates oriented to have opposite rubbing directions with respect to each other (Fig. 1d). The thickness of the LC cell set by a spherical spacer 20 μm in diameter was 21 ± 0.5 μm. The thickness was measured by the interference method by recording a transmission spectrum of an empty LC cell using an Ocean Optics USB4000 spectrometer (Ocean Insight, USA, California). The LC cell was assembled of two substrates with the dimensions of 15×10 mm. Liquid-crystalline suspensions were prepared using a nematic 4-pentyl-4'-cyanobiphenyl (5CB) and $BaTiO_3$ nanopowder (Nanotechcenter LLC, Ukraine) with a mean particle diameter of 24 nm. The nematic 5CB was synthesized at the "Institute of Single Crystals" (Kharkiv, Ukraine) and purified before use. We studied the LC suspensions with 0.5 and 1 wt.% of $BaTiO_3$ NPs added to the nematic 5CB. To obtain uniform distribution of $BaTiO_3$ NPs in the nematic 5CB, the suspension was subjected to room temperature sonication during 30 min using a UZDN-2T ultrasonic disperser (Ukrrospribor, Sumy, Ukraine) operating at the frequency of 22 kHz and providing the output power of 75 W. The LC cell was filled using a capillary method at a temperature higher than the isotropic transition temperature of 5CB (T_{Iso} = 308 K) to avoid additional aligning of LC molecules by the flow (see Figs. 1e and 1f).

2.2. Electrophysical measurements

The electric scheme for measuring steady state electric transport characteristics and transient processes in the studied samples is shown in Fig. 2. The electric voltage was applied to the sample with a series-connected resistor using a software-controlled voltage supply GW Instek PSP-603. To eliminate possible transient delays when measuring steady state current-voltage characteristics, the voltage magnitude was slowly varied at a rate of 20 mV per 5 s. Voltage drops on the sample with the load resistor were measured by Keithley-2000 digital multimeters and recorded by a control computer. An Aktakom ACK-3106 digital oscilloscope in the recorder mode was also used instead of the multimeters to record fast transients. To measure capacitance-voltage characteristics and capacitance values, RLC meters UNI-T UT612 (100, 120, 10^3, 10^4 and 10^5 Hz) and E7-12 (10^6 Hz) were used together with an external software-controlled dc voltage supply GW Instek PSP-603. Electrical contacts to the LC + $BaTiO_3$ cell were made by soldering indium onto the glass surface covered with an ITO layer.

The inset in Fig. 3 contains a transmission electron microscopy (TEM) image that shows the actual sizes and shapes of BTO NPs as well as presents some information about the spread of these parameters. As can be seen from this figure, the NPs may be regarded spherical in average. The average NP size (24 nm) and the size spread (from 17 to 47 nm) were determined in a conventional way [21]. The phase composition was determined by Rietveld refinement to be 7 wt.% of orthorhombic $BaCO_3$ and 93 wt.% of tetragonal $BaTiO_3$ [21].

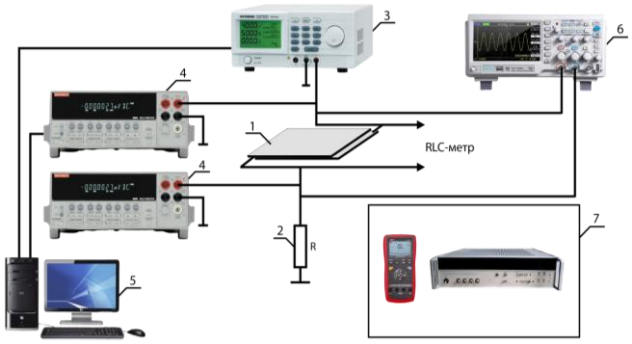

Fig. 2. Setup for measuring electrical characteristics: *1* – LC+BTO cell sample, *2* – load resistor for measuring current through the sample; *3* – voltage supply GW Instek PSP-603; *4* – Keithley 2000 digital multimeters, *5* – control and recording computer, *6* – digital oscilloscope Aktakom ACK-3106 for measuring fast transients, and *7* – RLC meters UNI-T UT612 and E7-12 for measuring capacity of the sample.

Current-voltage characteristics of the pure LC cells and the LC cells with 0.5 wt.% and 1.0 wt.% of BTO NPs measured in the dc regime are shown in Fig. 3. It can be seen from this figure that the empty LC cell demonstrates higher current values at the same voltage bias (and, hence, smaller resistance) as compared to the LC cells filled with a very small concentration (0.5 wt.%) of BTO NPs. Increase of the NPs concentration to 1 wt.% leads to further small decrease of the current especially at higher voltages. All the dc current-voltage characteristics shown in Fig. 3 manifest similar loop-like behavior, which is analyzed in more detail for one of them in Fig. 4.

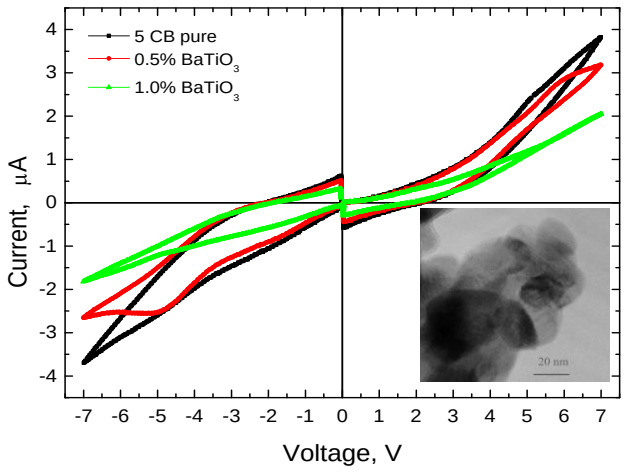

Fig. 3. Current-voltage characteristics of three LC cells with different concentrations of BTO NPs, measured at room temperature (300 K). Black loop: the cell with a pure LC 5CB (thickness of 20 μm, sample 1), red loop: the LC cell with 0.5 wt.% of BTO NPs (thickness of 20.7 μm, sample 2), green loop: the LC cell with 1.0 wt.% of BTO NPs (thickness of 20.6 μm, sample 3). A TEM image of the NPs is shown in the inset.

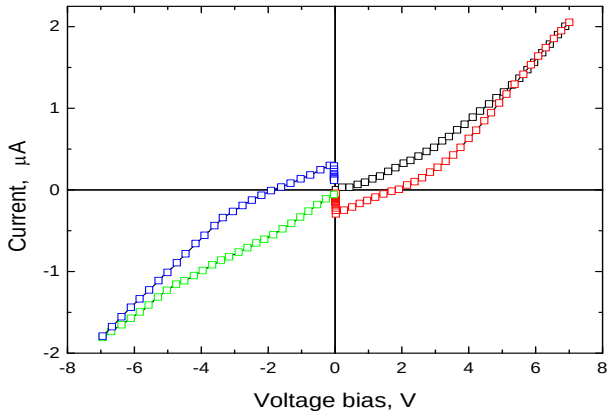

Fig. 4. Current-voltage characteristic of the LC cell with 1 wt.% of BTO NPs measured at 300 K. The black and green curves correspond to increasing the voltage bias in the forward and backward polarity, and the red and blue curves correspond to decreasing bias, respectively.

It can be seen from Fig. 4 that the direct current branches, shown by the black and green colors, start from zero current value at zero bias and exhibit a sub-linear or super-linear growth at increasing the voltage bias (at both bias polarities). The branches corresponding to the reverse voltage are shown by the red and blue colors. In these branches, the current decreases more rapidly at decreasing the voltage bias compared to the forward branches. A transition to the opposite current direction at certain voltage is observed. At zero voltage provided by the power supply, an opposite-sign voltage of the level of about 3 mV is registered on the sample. This effect evidences the remaining opposite sign polarization of the sample corresponding to the electric field of about 1.5 V/cm. The sample remained unbiased for about 10 minutes after reducing the bias down to 0 to discharge it through a 10 kOhm load resistor. After the current decreased to zero, the loop was recorded at applied bias of the opposite sign. In general, this loop almost repeated the initial loop shape.

The same trend is observed for the charge-voltage characteristics. Namely, the capacitance loop is the widest for the empty LC cell and becomes noticeably thinner in the presence of 0.5 and 1 wt.% of BTO NPs (see Fig. 5). This seems counterintuitive, because 1 wt.% of the NPs modifies the dielectric constant of the mixture very slightly. A possible physical reason of this observation is the influence of ionic-electronic screening charges and dielectrophoretic forces (which are very weak but at the same time long-range and omnipresent) on the ionic transport in the LC.

In contrast to the current-voltage characteristics, the capacitance *vs* voltage bias curves (except the feature mentioned above) have an antisymmetric shape in regard of polarity change. The capacitance keeps its value close to that at zero bias in the bias range of –4 to +4 V. At higher bias, which corresponds to the field above 2 kV/cm, the capacitance sharply decreases by two times

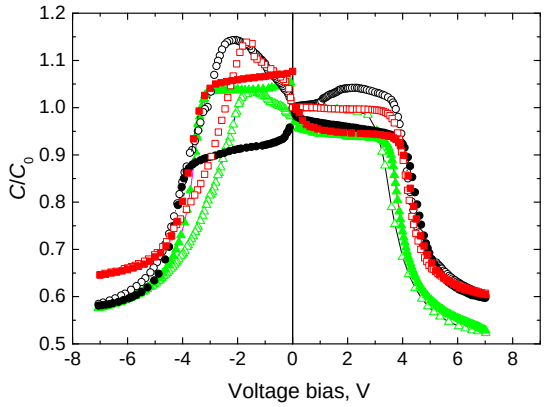

Fig. 5. C/C_0 (C being the capacitance and C_0 being the zero-bias capacitance, respectively) *vs* bias voltage on the LC cell with BTO NPs measured at room temperature (300 K). Black circles correspond to the cell with a pure LC 5CB (thickness of 20 μm, sample 1), red squares correspond to the LC cell with 0.5 wt.% of BTO NPs (thickness of 20.7 μm, sample 2), green triangles correspond to the LC cell with 1.0 wt.% of BTO NPs (thickness of 20.6 μm, sample 3). Empty symbols correspond to increasing bias and filled symbols correspond to decreasing bias.

and then tends to saturation. Such behavior is typical *e.g.* for a situation when a fraction of the space charge contributing to slow polarization is eliminated by a strong electric field.

The frequency dependences of the dielectric permittivity and losses of the pure LC cell and the LC cells with 0.5 and 1 wt.% of BTO NPs are shown Figs. 6a and 6b, respectively. As can be seen from Fig. 6a, the dielectric permittivity of all the samples monotonously decreases at increasing frequency in the whole range from 100 Hz to 1 MHz. In the frequency range of 10^2 to 10^5 Hz, the decrease is slow, while a quick decrease is observed at higher frequencies. The capacitance of the pure LC cell is the smallest. The capacitance values of the LC cell with 0.5 and 1 wt.% of BTO NPs coincide with each other in the entire frequency range. The weak increase of the low-frequency permittivity upon adding BTO NPs qualitatively agrees with the Maxwell–Garnett effective media approximation. Fast decrease in the permittivity is observed for the frequencies above 0.1 MHz. All the permittivity curves merge in the frequency range of 10^2 to 10^5 Hz. The significant (by 10 times) decrease in the capacitance with the increase in frequency by 4 orders of magnitude is inherent to ion motion in the LC and is hardly possible in wide-gap ferroelectric materials.

As can be seen from Fig. 6b, the losses of the pure LC cell and LC cells with 0.5 and 1 wt.% of BTO NPs vary non-monotonously, first decreasing with the frequency increase from 10^2 to 10^4 Hz and then increasing with frequency. At 10^4 Hz, the losses of all the cells reach the absolute minima. In general, the dependences of the losses angle tangent on the frequency are very close to each other, which evidences the prevailing contribution of the LC matrix. While the decreasing with

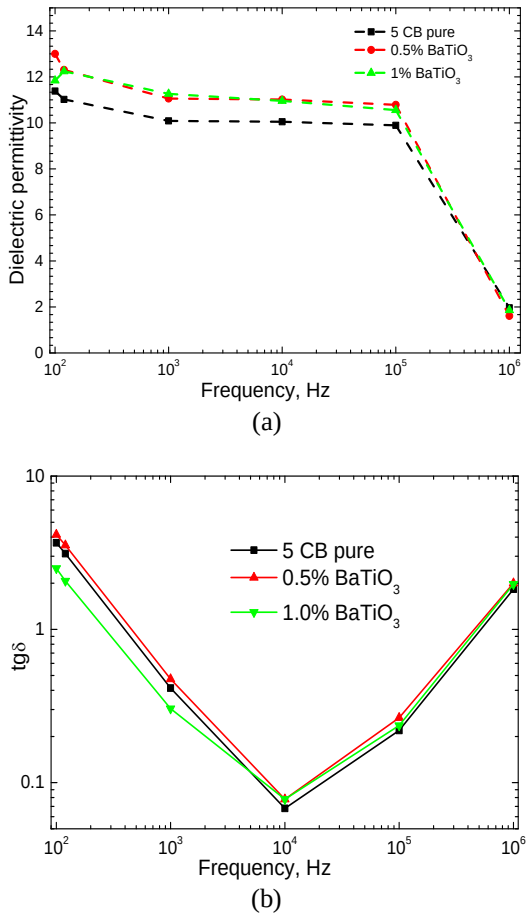

Fig. 6. Effective dielectric permittivity (a) and losses angle tangent tgδ (b) of the LC cells with BTO NPs measured at room temperature (300 K). The sample description is the same as in Fig. 3.

frequency part may be related to a decreasing ratio of the real and imaginary components of complex impedance, the increasing part at higher frequencies may be related to the retarding effects in the screened particles.

We also measured current-voltage characteristics in the frequency range of 10 Hz…1 kHz using a triangular-shaped applied voltage profile. The current-voltage characteristics correspond to a linear RC circuit at 1 kHz, an RC circuit with a very small nonlinearity at 100 Hz, and an RC circuit with more pronounced nonlinearity (Rayleigh bi-angle-like loop shape) at 10 Hz. The multiplicity of the resistance increase is (1.3…2) times and is maximal for the 5CB with 1 wt.% of BTO NPs, the resistance of which is maximal. The capacitance increase is much greater than the increase of the resistance; and the capacity increase is maximal (~ 10 times) under the frequency increase from 100 Hz to 10 kHz. This result agrees well with the conclusion that slow dynamics of the ionic-electronic charge, which screens the ferroelectric NPs and/or is accumulated near the electrodes, determines the nonlinear features of the current-voltage curves of the LC cell with or without ferroelectric NPs.

3. Theoretical model

It is also well known that small NPs (with sizes less than 10…50 nm) at the concentrations less than 1 wt.% cannot change the director distribution and/or elastic properties of LC in a noticeable way. Hence, the small concentrations of the NPs cannot directly influence on the current-voltage and charge-voltage characteristics of the LC cells. However, the above-presented experimental results reveal an apparent influence of the ultra-small concentrations of the BTO NPs (1 wt.% or less) on the electrophysical properties and effective capacitance of the dielectric LC 5CB. A possible physical reason of this observation is the indirect influence on the slow ionic transport in LC of the screening charges, which cover the ferroelectric NPs and become polarized in the external field. We use the effective media approximation below to calculate the effective capacitance of the LC 5CB and colloid LC 5CB with BTO NPs.

A. Effective media approximation

There are many effective media approximations (EMA) [26], among which the Landau approximation of a linear mixture [27], Maxwell–Garnett [28] and Bruggeman [29] approximations for spherical inclusions, and Lichtenecker–Rother approximation of a logarithmic mixture [30] are the most known. Most of these approximations are applicable to quasi-spherical randomly distributed dielectric (or semiconducting) particles in an insulating environment. These EMA models provide explicit expressions for the effective permittivity ε^*_{eff}. However, their applicability ranges are very sensitive to the cross-interaction effects of the polarized NPs, and, therefore, most of them can be invalid for dense composites and/or colloids, where the volume fraction of ferroelectric particles exceeds 20…30%.

One of the effective media approximations was proposed by Carr *et al*. [31]. This EMA was successfully used by Petzelt *et al*. [32] and Rychetský *et al*. [33]. It provides a quadratic equation for the effective permittivity of a binary mixture:

$$(1-\mu)\frac{\varepsilon^*_{eff}-\varepsilon^*_b}{(1-n_a)\varepsilon^*_{eff}+n_a\varepsilon^*_b}+\mu\frac{\varepsilon^*_{eff}-\varepsilon^*_a}{(1-n_a)\varepsilon^*_{eff}+n_a\varepsilon^*_a}=0\,. \quad (1)$$

Here, ε^*_a, ε^*_b are the relative complex permittivities of the components "*a*" and "*b*", respectively, μ and $(1-\mu)$ are the relative volume fractions of these components, and n_a is the depolarization field factor for an inclusion of the type "*a*", respectively.

Using the EMA for $\mu << 1$ (and, hence, $\varepsilon^*_{eff} \approx \varepsilon^*_b$) we derived the following linearized equation for the effective permittivity ε_{eff} [34]:

$$\varepsilon^*_{eff}=\varepsilon^*_b\left[1+\frac{\mu(\varepsilon^*_a-\varepsilon^*_b)}{n_a\varepsilon^*_a+(1-n_a)\varepsilon^*_b-n_a\mu(\varepsilon^*_a-\varepsilon^*_b)}\right]. \quad (2a)$$

We supposed here that the external electric field is directed along one of the principal axes of the ellipsoidal particles, for which the depolarization factor is n_a. Eq. (2a) contains the term $-n_a\mu(\varepsilon^*_a-\varepsilon^*_b)$ in the denominator, which makes it more consistent with the solution of the EMA equation (1). Similar expression (but without the mentioned term) was derived by Hudak *et al*. [35].

Eq. (2a) contains the first two terms of an expansion of the effective permittivity (1) with respect to μ. For an adequate study of an anisotropic liquid, such as a liquid crystal, as a surrounding medium, the effects of anisotropy of ε_e, which can be rather strong (see *e.g*. [36, 37]),

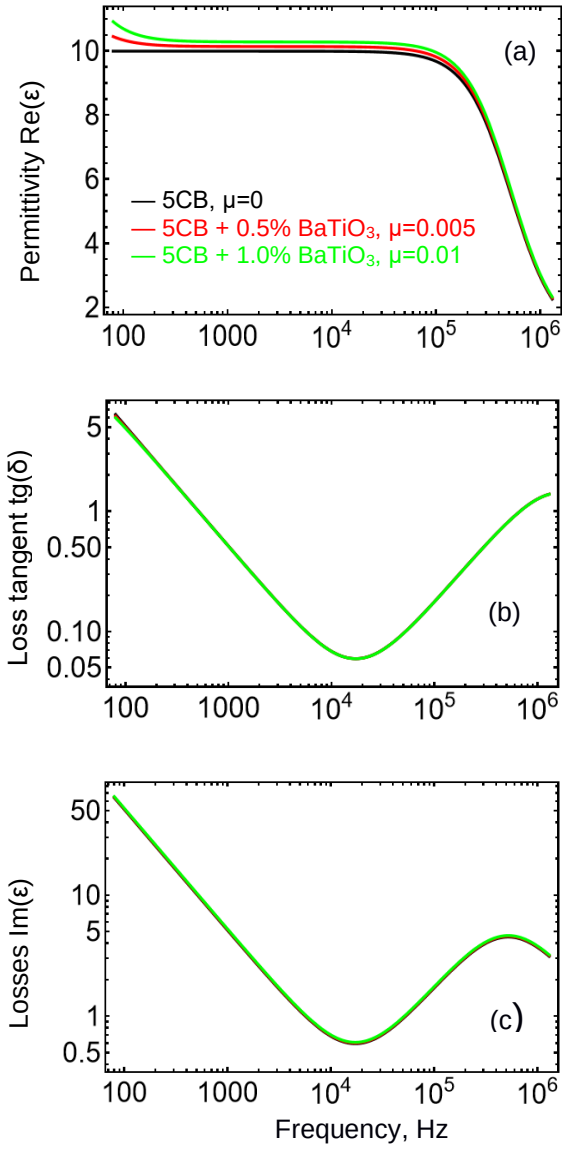

Fig. 7. Frequency dependences of the real part of dielectric permittivity (a), losses angle tangent tgδ (b), and imaginary part of dielectric permittivity (c), calculated from Eqs. (2) for n_a = 0.33, ε_a = 500, σ_a = 1 s^{-1}, ε_∞ = 1, ε_b = 10, $\tau = 1.91\cdot10^{-6}$ s, and $\sigma_b = 5.1\cdot10^{3}$ s^{-1}. Here, the relative volume fraction for the pure LC 5 CB is μ = 0, μ = 0.005 for the LC cell with 0.5% of BTO NPs, and μ = 0.01 for the LC cell with 1.0% of BTO NPs.

should be considered. We assume next that the NPs have the complex dielectric permittivity $\varepsilon_a^* = \varepsilon_a - i\frac{\sigma_a}{\omega}$ and the LC has the complex permittivity

$$\varepsilon_b^* = \varepsilon_\infty + \frac{\varepsilon_b - \varepsilon_\infty - i\frac{\sigma_b}{\omega}}{1 + i\tau\omega}. \quad (2b)$$

The LC 5CB parameters can be found in [38].

Frequency dependences of the real part of the dielectric permittivity $\mathrm{Re}\left(\varepsilon_{eff}^*\right)$, losses angle tangent tg δ, and losses $\mathrm{Im}\left(\varepsilon_{eff}^*\right)$ are shown in Figs. 7a–7c. The dependences are calculated by Eqs. (2) with $n_a = 0.33$, $\varepsilon_a = 500$, $\varepsilon_\infty = 1$, and $\varepsilon_b = 10$. The values of the parameters $\sigma_a = 1\ \mathrm{s}^{-1}$, $\tau = 1.91\cdot10^{-6}$ s and $\sigma_b = 5.1\cdot10^{3}\ \mathrm{s}^{-1}$ were determined from the best agreement with the experimental dependences shown in Fig. 6.

The calculated frequency dependences of the real part of the dielectric permittivity quantitatively agree with the respective experimentally measured dependences (compare Fig. 6a and Fig. 7a). The effective permittivity of the LC cell with 1.0% of BTO NPs is slightly higher than that of the LC cell with 0.5% of BTO NPs, and the latter is slightly higher than the permittivity of the pure LC 5CB (compare the green, red and black curve in Fig. 7a).

The calculated frequency dependences of the tgδ semi-quantitatively agree with the respective experimentally measured dependences (compare Fig. 6b and Fig. 7b). The tgδ of the LC cell with 1.0% of BTO NPs, the LC cell with 0.5% of BTO NPs, and the pure LC 5CB coincide (compare the green, red and black curve in Fig. 7b). The tgδ reaches the minimum near 20 kHz. The parameters $\sigma_b >> \sigma_a$ and τ determine the frequency position of the minimum. The minimum is very weakly sensitive to the parameters σ_a (until $\sigma_a << \sigma_b$), ε_a and ε_b.

The calculated frequency dependences of the losses in the LC cell with 1.0% of BTO NPs, the LC cell with 0.5% of BTO NPs, and the pure LC 5CB coincide (compare the green, red and black curve in Fig. 7c).

4. Conclusions

We reveal an apparent influence of very small concentrations (1 wt.% or less) of $BaTiO_3$ NPs (average size of 24 nm) on the current-voltage characteristics and capacitance of LC 5CB. The pure LC cell demonstrates higher current (and, hence, smaller resistance) as compared to the LC cells filled with 0.5 and 1 wt.% of BTO NPs. The same trend is observed for the charge-voltage characteristics. The capacitance loop is the widest for the pure LC cell and becomes noticeably thinner in the presence of 0.5 and 1 wt.% of BTO NPs. This seems unusual, because 1 wt.% of NPs modifies the effective dielectric constant very slightly and practically has no influence on the director distribution and elastic properties of the LC.

A possible physical reason of this observation is the influence on the slow ionic transport in the LC of the screening charges, which cover the ferroelectric NPs and become polarized in an external field. To quantify the experimental results, we calculate the effective dielectric permittivity and losses for an ensemble of NPs in liquid dielectric media in the effective media approximation. The results of the analytical calculations are in a semi-quantitative agreement with the experimental results. The obtained results can be used to tailor metamaterials for multiple practical applications.

Acknowledgements

The work of J.M.G, O.S.P., E.A.E. and A.N.M. is supported by the National Research Foundation of Ukraine (project "Manyfold-degenerated metastable states of spontaneous polarization in nanoferroics: theory, experiment and perspectives for digital nanoelectronics", grant No. 2023.03/0132, and project "Silicon-compatible ferroelectric nanocomposites for electronics and sensors", grant No. 2023.03/0127). The work of V.V.V., D.O.S., N.V.M. and V.N.P. is supported by the Target Program of the National Academy of Sciences of Ukraine, Project No. 5.8/25-П "Energy-saving and environmentally friendly nanoscale ferroics for the development of sensorics, nanoelectronics and spintronics". The materials preparation and characterization (S.E.I.) is sponsored by the NATO Science for Peace and Security Programme under the grant SPS G5980 "FRAPCOM".

References

1. Reznikov Y., Buchnev O., Tereshchenko O. *et al.* Ferroelectric nematic suspension. *Appl. Phys. Lett*. 2003. **82**, No 12. P. 1917–1919. https://doi.org/10.1063/1.1560871.
2. Atkuri H., Cook G., Evans D.R. *et al.* Preparation of ferroelectric nanoparticles for their use in liquid crystalline colloids. *J. Opt. A: Pure Appl. Opt.* 2009. **11**, No 2. P. 024006. https://doi.org/10.1088/1464-4258/11/2/024006.
3. Kurochkin O., Atkuri H., Buchnev O. *et al.* Nano-colloids of $Sn_2P_2S_6$ in nematic liquid crystal pentyl-cianobiphenile. *Condens. Matter Phys.* 2010. **13**, No 3. P. 33701(1–9). https://doi.org/10.5488/CMP.13.33701.
4. Caruntu D., Rostamzadeh T., Costanzo T. *et al.* Solvothermal synthesis and controlled self-assembly of monodisperse titanium-based perovskite colloidal nanocrystals. *Nanoscale*. 2015. **7**, No 30. P. 12955. https://doi.org/10.1039/C5NR00737B.
5. Nayak S., Chaki T.K., Khastgir D. Spherical ferroelectric $PbZr_{0.52}Ti_{0.48}O_3$ nanoparticles with high permittivity: Switchable dielectric phase transition with temperature. *Ceram. Int*. 2016. **42**. P. 14490. https://doi.org/10.1016/j.ceramint.2016.06.056.
6. Cook G., Glushchenko A.V., Reshetnyak V. *et al.* Nanoparticle doped organic-inorganic hybrid photorefractives. *Opt. Expess*. 2008. **16**, No 6. P. 4015. https://doi.org/10.1364/OE.16.004015.

7. Evans D.R., Basun S.A., Cook G. *et al.* Electric field interactions and aggregation dynamics of ferroelectric nanoparticles in isotropic fluid suspensions. *Phys. Rev. B.* 2011. **84**, No 17. P. 174111. https://doi.org/10.1103/PhysRevB.84.174111.
8. Lorenz A., Zimmermann N., Kumar S. *et al.* Doping the nematic liquid crystal 5CB with milled $BaTiO_3$ nanoparticles. *Phys. Rev. E*. 2012. **86**. P. 051704. https://doi.org/10.1103/PhysRevE.86.051704.
9. Beh E.S., Basun S.A., Feng X. *et al.* Molecular catalysis at polarized interfaces created by ferroelectric $BaTiO_3$. *Chem. Sci*. 2017. **8**, No 4. P. 2790. https://doi.org/10.1039/C6SC05032H.
10. Cook G., Barnes J.L., Basun S.A. *et al.* Harvesting single ferroelectric domain stressed nanoparticles for optical and ferroic applications. *J. Appl. Phys.* 2010. **108**, No 6. P. 064309. https://doi.org/10.1063/1.3477163.
11. Basun S.A., Cook G., Reshetnyak V.Y. *et al.* Dipole moment and spontaneous polarization of ferroelectric nanoparticles in a nonpolar fluid suspension. *Phys. Rev. B*. 2011. **84**. P. 024105. https://doi.org/10.1103/PhysRevB.84.024105.
12. Starzonek S., Rzoska S.J., Drozd-Rzoska A. *et al.* Impact of ferroelectric and superparaelectric nanoparticles on phase transitions and dynamics in nematic liquid crystals. *Phys. Rev. E*. 2017. **96**. P. 022705. https://doi.org/10.1103/PhysRevE.96.022705.
13. Mertelj A., Cmok L., Čopič M. *et al.* Critical behavior of director fluctuations in suspensions of ferroelectric nanoparticles in liquid crystal at nematic to SmA phase transition. *Phys. Rev. E*. 2010. **85**. P. 021705. https://doi.org/10.1103/PhysRevE.85.021705.
14. Lorenz A., Zimmermann N., Kumar S. *et al.* Doping a mixture of two smectogenic liquid crystals with barium titanate nanoparticles. *J. Phys. Chem. B*. 2013. **117**, No 3. P. 937. https://doi.org/10.1021/jp310624c.
15. Shukla R.K., Liebig C.M., Evans D.R., Haase W. Electro-optical behavior and dielectric dynamics of harvested ferroelectric $LiNbO_3$ nanoparticles doped ferroelectric liquid crystal nanocolloids. *Royal Society of Chemistry, RSC Adv*. 2014. **36**. P. 18529. https://doi.org/10.1039/C4RA00183D.
16. Idehenre I.U., Barnakov Yu.A., Basun S.A., Evans D.R. Spectroscopic studies of the effects of mechanochemical synthesis on $BaTiO_3$ nanocolloids prepared using high-energy ball-milling. *J. Appl. Phys.* 2018. **124**. P. 165501. https://doi.org/10.1063/1.5046682.
17. Barnakov Y.A., Idehenre I.U., Basun S.A. *et al.* Uncovering the mystery of ferroelectricity in zero dimensional nanoparticles. *Nanoscale Adv*. 2019. **2.** P. 664. https://doi.org/10.1039/C8NA00131F.
18. Eliseev E.A., Morozovska A.N., Vysochanskii Y.M. *et al.* Light-induced transitions of polar state and domain morphology in photo-ferroelectric nanoparticles. *Phys. Rev. B*. 2024. **109.** P. 045434. https://doi.org/10.1103/PhysRevB.109.045434.
19. Zhang H., Liu S., Ghose S. *et al.* Structural origin of recovered ferroelectricity in $BaTiO_3$ nanoparticles. *Phys. Rev. B*. 2023. **108**. P. 064106. https://doi.org/10.1103/PhysRevB.108.064106.
20. Eliseev E.A., Morozovska A.N., Kalinin S.V., Evans D.R. Strain-induced polarization enhancement in $BaTiO_3$ core-shell nanoparticles. *Phys. Rev. B*. 2024. **109**. P. 014104. https://doi.org/10.1103/PhysRevB.109.014104.
21. Morozovska A., Pylypchuk O., Ivanchenko S. *et al.* Electrocaloric response of the dense ferroelectric nanocomposites. *Ceramics Int.* 2024. **50**. P. 11743. https://doi.org/10.1016/j.ceramint.2024.01.079.
22. Silibin M.V., Solnyshkin A.V., Kiselev D.A. *et al.* Local ferroelectric properties in PVDF/BPZT nanocomposites: Interface effect. *J. Appl. Phys.* 2013. **114**. P. 144102. https://doi.org/10.1063/1.4824463.
23. Silibin M., Belovickis J., Svirskas S. *et al.* Polarization reversal in organic-inorganic ferroelectric composites: modeling and experiment. *Appl. Phys. Lett.* 2015. **107**. P. 142907. https://doi.org/10.1063/1.4932661.
24. Yang F.Z., Cheng H.F., Gao H.J. *et al.* Technique for characterizing azimuthal anchoring of twisted nematic liquid crystals using half-leaky guided modes. *J. Opt. Soc. Am. B*. 2001. **18**, No 7. P. 994–1002. https://doi.org/10.1364/JOSAB.18.000994.
25. HD MicroSystems Product bulletin PI2525, PI2555 and PI2574; 2012 Nov.
26. Choy T.C. *Effective Medium Theory*. Oxford: Clarendon Press, 1999.
27. Landau L.D., Pitaevskii L.P., Lifshitz E.M. *Electrodynamics of Continuous Media*. **8**. Elsevier, 2013.
28. Garnett J.C.M. Colours in metal glasses and in metallic films. *Phil. Trans. R. Soc. London. Ser. A*. 1904. **203**. P. 385. https://doi.org/10.1098/rsta.1904.0024.
29. Bruggeman D.A.G. Berechnung verschiedener physikalischer Konstanten von heterogenen Substanzen. I. Dielektrizitätskonstanten und Leitfähigkeiten der Mischkörper aus isotropen Substanzen. *Ann. Phys.* 1935. **416**. P. 636. https://doi.org/10.1002/andp.19354160705.
30. Simpkin R. Derivation of Lichtenecker's logarithmmic mixture formula from Maxwell's equations. *IEEE Trans. Microw. Theory Techn*. 2010. **58.** P. 545. https://doi.org/10.1109/TMTT.2010.2040406.
31. Carr G.L., Perkowitz S., Tanner D.B. Far-infrared properties of inhomogeneous materials. In: *Infrared and Millimeter Waves*. Vol. 13, ed. K.J. Button. Academic Press, Orlando, 1985. P. 171–263.
32. Petzelt J., Nuzhnyy D., Bovtun V., Crandles D.A. Origin of the colossal permittivity of (Nb+In) co-doped rutile ceramics by wide-range dielectric spectroscopy. *Phase Trans.* 2018. **91.** P. 932. https://doi.org/10.1080/01411594.2018.1501801.
33. Rychetský I., Nuzhnyy D., Petzelt J. Giant permittivity effects from the core–shell structure modeling of the dielectric spectra. *Ferroelectrics.* 2020. **9**. P. 569. https://doi.org/10.1080/00150193.2020.1791659.

34. Pylypchuk O.S., Ivanchenko S.E., Yelisieiev M.Y. *et al.* Behavior of the dielectric and pyroelectric responses of ferroelectric fine-grained ceramics. *J. Am. Ceram. Soc*. 2025. https://doi.org/10.1111/e20391.
35. Hudak O., Rychetsky I., Petzelt J. Dielectric response of microcomposite ferroelectrics. *Ferroelectrics*. 1998. **208–209**. P. 429–447. https://doi.org/10.1080/00150199808014891.
36. Shelestiuk S.M., Reshetnyak V.Yu., Sluckin T.J. Frederiks transition in ferroelectric liquid-crystal nanosuspensions. *Phys. Rev. E*. 2011. **83**. P. 041705. https://doi.org/10.1103/PhysRevE.83.041705.
37. Al-Zangana S., Iliut M., Turner M. *et al.* Properties of a thermotropic nematic liquid crystal doped with graphene oxide. *Adv. Opt. Mater*. 2016. **4**. P. 1541. https://doi.org/10.1002/adom.201600351.
38. Bogi A., Faetti S. Elastic, dielectric and optical constants of 4'-pentyl-4-cyanobiphenyl. *Liquid Crystals*. 2001. **28**, No 5. P. 729–739. https://doi.org/10.1080/02678290010021589.

Authors and CV

Juliya Mykolayivna Gudenko, born in 1982, PhD in Physics and Mathematics (Solid State Physics, 2015), Researcher at the Department of Solid State Electronics, Institute of Physics. Author of more than 10 scientific publications. The area of her scientific interests includes transport properties of low-dimensional semiconductor structures and nanoscale materials.
E-mail: Gudenko.juliya@gmail.com,
https://orcid.org/0009-0005-5938-5480

Oleksandr Sergiyovych Pylypchuk, born in 1986, PhD in Physics and Mathematics (Solid State Physics, 2015), Senior Researcher at the Department of Solid State Electronics, Institute of Physics. Author of more than 40 scientific publications. The area of his scientific interests includes transport properties of low-dimensional semiconductor structures and nanoscale materials.
E-mail: pylypchuk@iop.kiev.ua,
https://orcid.org/0000-0003-0136-0799

Denis Olegovych Stetsenko, born in 1994. PhD student. He is an Engineer at the Department of Physics of Magnetic Phenomena, Institute of Physics. The area of his scientific interests includes magnetic phenomena in solids. E-mail: wh.denis.stetsenko@gmail.com,
https://orcid.org/0009-0002-9141-0939

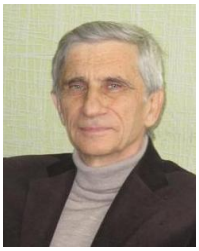

Viktor Volodymyrovich Vainberg, born in 1951. Doctor of Sciences in Physics and Mathematics (Solid State Physics, 2015), Leading Researcher at the Department of Solid State Electronics, Institute of Physics. Author of more than 100 scientific publications. His current research trend is transport properties of low-dimensional semiconductor structures and nanoscale materials.
E-mail: viktor.vainberg@gmail.com,
https://orcid.org/0000-0002-9840-8033

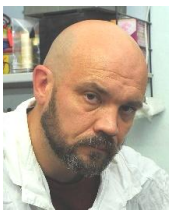

Igor Anatoliyovych Gvozdovskyy, born in 1975. PhD in Physics and Mathematics (Molecular and Liquid Crystal Physics, 2004), Senior Researcher at the Department of Optical Quantum Electronics, Institute of Physics. Author of 51 scientific publications (nowadays 40 of them are indexed in the SCOPUS database). The area of his interests is blue phases of pure cholesteric liquid crystals doped by photosensitive chiral dopants, reactive mesogen monomers and various nanoparticle types. In recent years, he studies chiral nematic twist-bend (N^*_{tb}) and chiral nematic ferroelectric (N^*_F) phases. E-mail: igvozd@gmail.com,
https://orcid.org/0000-0002-4531-9942

Serhii Eduardovych Ivanchenko, born in 1989. PhD in Engineering Science (2023). Researcher at the Department of Physical Chemistry and Technology of Nanostructured Ceramics and Nanocomposites, Frantsevich Institute for Problems of Materials Science. Author of more than 50 scientific publications. The areas of his scientific interest include rheology, powder metallurgy, tape casting, polymer-ceramic composites, and multilayer composites.
E-mail: s.ivanchenko@ipms.kyiv.ua,
sergonische@gmail.com,
https://orcid.org/0000-0002-9859-1835

Vladimir Nikolayevich Poroshin, born in 1951. Doctor of Sciences in Physics and Mathematics (2006), Deputy Director of Research, Institute of Physics, Head of the Department of Solid State Electronics. Authored more than 100 publications. The area of his scientific interests includes fundamental research of electron and phonon transport phenomena, magneto-transport of carriers in bulk semiconductors and quantum heterostructures, effects of light absorption and emission by hot carriers.
E-mail: poroshin@iop.kiev.ua,
https://orcid.org/0000-0001-8217-3949

Eugene Anatolievich Eliseev, born in 1977. PhD in Solid State Physics (2003), Doctor of Sciences in Solid State Physics (2009), Senior Researcher (2015), Head of the Department of Functional Oxide Materials, Department of Solid State Electronics, Institute of Physics. Author of more than 350 scientific publications. The area of his scientific interests is theory of ferroics and phase diagrams, mixed ionic-electronic conductors and related materials.
E-mail: eugene.a.eliseev@gmail.com,
https://orcid.org/0000-0001-8124-8857

Anna Nikolaevna Morozovska, born in 1977, PhD in Optics and Laser Physics (2004), Doctor of Sciences in Solid State Physics (2009), Professor in Physics and Astronomy (2023), Leading Scientific Researcher at the Department of Physics of Magnetic Phenomena at the Institute of Physics. Author of more than 400 scientific publications. The area of her scientific interests is theory of ferroics and multiferroics, mixed ionic-electronic conductors and related materials.
E-mail: anna.n.morozovska@gmail.com,
https://orcid.org/0000-0002-8505-458X

Nicholas Vladimirovich Morozovsky, born in 1949. Doctor of Sciences in Solid State Physics (1996), Leading Researcher at the Laboratory of Applied Ferroelectrics of the Institute of Physics. The area of his scientific interests includes ferroelectricity and pyroelectricity, and thermos-wave probing.
E-mail: nicholas.v.morozovsky@gmail.com,
https://orcid.org/0000-0003-2937-4850

Authors' contributions

Gudenko Ju.M.: visualization, investigation, formal analysis, writing – review & editing.
Pylypchuk O.S.: visualization, investigation, formal analysis, methodology, writing – original draft, review & editing.
Vainberg V.V.: validation, methodology, conceptualization, writing – review & editing.
Gvozdovskyy I.A.: investigation, resources.
Ivanchenko S.E.: resources.
Stetsenko D.O.: investigation, resources.
Morozovsky N.V.: investigation.
Poroshin V.N.: validation, conceptualization, data curation.
Eliseev E.A.: methodology, validation, formal analysis.
Morozovska A.N.: formal analysis, conceptualization, methodology, writing – original draft, review & editing.

Сегнетоелектричні наночастинки в рідких кристалах: роль іонного транспорту при малих концентраціях наночастинок

Ю.М. Гуденко, О.С. Пилипчук, В.В. Вайнберг, І.А. Гвоздовський, С.Е. Іванченко, Д.О. Стеценко, М.В. Морозовський, В.М. Порошин, Є.А. Єлісєєв, та Г.М. Морозовська

Анотація. Виявлено значний вплив надмалих концентрацій (1 мас. % або менше) наночастинок $BaTiO_3$ (BTO, середній розмір 24 нм) на вольт-амперні характеристики та ємність діелектричного рідкого кристала (РК) 5 CB. Чиста РК комірка пропускає більший струм (а, отже, має менший опір) порівняно з РК комірками, які містять наночастинки BTO з дуже малими концентраціями (0,5 та 1 мас.%). Така ж тенденція спостерігається і для вольт-фарадних характеристик: петля ємності є найширшою для чистої РК комірки та помітно тоншає за наявності наночастинок $BaTiO_3$ з 0,5 та 1 мас.%. Такі результати є неочікуваними, оскільки сегнетоелектричні наночастинки з 1 мас.% незначно змінюють ефективний діелектричний відгук і тому не повинні впливати на розподіл директора та пружні властивості РК. Таким чином, можливою фізичною причиною цього спостереження є вплив на іонний транспорт у РК іонно-електронних екрануючих зарядів, які включають сегнетоелектричні наночастинки та поляризуються у зовнішньому полі.

Ключові слова: діелектричний рідкий кристал, сегнетоелектричні наночастинки, наночастинки $BaTiO_3$, вольт-амперні характеристики, іонний транспорт.